

1 Stratospheric ozone depletion inside the volcanic plume shortly after the 2 2022 Hunga Tonga eruption

3
4 Yunqian Zhu^{1,2,3}, Robert W. Portmann¹, Douglas Kinnison⁴, Owen Brian Toon^{3,5}, Luis Millán⁶,
5 Jun Zhang⁴, Holger Vömel⁷, Simone Tilmes⁴, Charles G. Bardeen⁴, Xinyue Wang⁴, Stephanie
6 Evan⁸, William J. Randel⁴, Karen H. Rosenlof¹

- 7
- 8 1. NOAA, Chemical Sciences Laboratory
- 9 2. Cooperative Institute for Research in Environmental Sciences, University of Colorado
10 Boulder
- 11 3. Laboratory for Atmospheric and Space Physics, University of Colorado Boulder
- 12 4. NCAR, Atmospheric Chemistry Observations and Modeling Laboratory
- 13 5. Department of Atmospheric and Oceanic Sciences, University of Colorado Boulder
- 14 6. Jet Propulsion Laboratory, California Institute of Technology, 4800 Oak Grove Drive,
15 Pasadena, CA 91109, USA
- 16 7. NCAR, Earth Observing Laboratory
- 17 8. Laboratoire de l'Atmosphère et des Cyclones (LACy, UMR8105, CNRS, Université de La
18 Réunion, Météo-France), Saint-Denis, France

19
20 Corresponding author: Yunqian Zhu (yunqian.zhu@noaa.gov)

21 22 **Abstract**

23 Near-term in-plume ozone depletion was observed for about ten days by Microwave Limb
24 Sounder (Aura/MLS) right after the January 2022 Hunga Tonga-Hunga Ha'apai (HTHH)
25 eruption. This work analyzes the dynamic and chemical causes of this ozone depletion. The
26 results show that the large water injection (~ 150 Tg) from the HTHH eruption, with ~ 0.0013 Tg
27 injection of ClO (or ~ 0.0009 Tg of HCl), causes ozone loss due to strongly enhanced HOx and
28 ClOx cycles and their interactions. Aside from the gas phase chemistry, the heterogeneous
29 reaction rate for $\text{HOCl} + \text{HCl} \rightarrow \text{Cl}_2 + \text{H}_2\text{O}$ increases to $10^4 \text{ cm}^{-3} \text{ sec}^{-1}$ and is a major cause of
30 chlorine activation, making this event unique compared with the springtime polar ozone
31 depletion where $\text{HCl} + \text{ClONO}_2$ is more important. The large water injection causes relative
32 humidity over ice to increase to 70% - 100%, decreases the $\text{H}_2\text{SO}_4/\text{H}_2\text{O}$ binary solution weight
33 percent to 35% compared with the 70% ambient value, and decreases the plume temperature by
34 2-6 K. These changes lead to high heterogeneous reaction rates. Plume lofting of ozone-poor air
35 is evident during the first two days after the eruption, but ozone concentrations quickly recover
36 because its chemical lifetime is short at 20 hPa. With such a large seawater injection, we expect
37 that ~ 5 Tg Cl was lifted into the stratosphere by the HTHH eruption in the form of NaCl, but
38 only $\sim 0.02\%$ of that remained as active chlorine in the stratosphere. Lightning NOx changes are
39 probably not the reason for the HTHH initial in-plume O_3 loss.

40 41 **Key points:**

- 42 ● HOCl is identified as playing a large role in the in-plume chlorine balance and
43 heterogeneous processes, making this event unique compared with the ozone hole where
44 $\text{HCl} + \text{ClONO}_2$ is more important.
- 45 ● The HTHH eruption enhanced the HOx/ClOx cycles and their interactions, which caused
46 in-plume O_3 depletion.

- The injection of Cl, H₂O, and lightning NO_x modified the ambient chemistry.

Plane Text Summary

The 2022 Hunga Tonga eruption injected a large amount of water into the stratosphere. Ozone depletion was observed inside the volcanic plume. Chlorine and water vapor injected by this eruption exceeded the normal range, which made the ozone chemistry during this event occur at a higher temperature than polar ozone depletion. Unlike polar ozone chemistry where chlorine nitrate is more important, hypochlorous acid plays a large role in the in-plume chlorine balance and heterogeneous processes.

1. Introduction

Stratospheric ozone concentrations change after volcanic eruptions for a variety of reasons. Enhanced polar ozone depletion occurs after large or medium volcanic eruptions [Hofmann and Oltmans, 1993; Portmann *et al.*, 1996; Solomon *et al.*, 2016] since heterogeneous reactions on volcanically enhanced sulfate aerosols result in amplified anthropogenic ClO_x and BrO_x induced ozone loss. Tie and Brasseur [1995] demonstrated that mid- and high latitude O₃ changes after a volcanic eruption largely depend on chlorine loading. For the pre-industrial era and in the absence of anthropogenic halogens in the stratosphere, O₃ would slightly increase in the middle atmosphere after a large volcanic eruption resulting from the suppression of NO_x-catalyzed destruction by heterogeneous creation of HNO₃ on volcanic aerosols. After the 1991 Pinatubo eruption, the radiative heating caused by volcanic aerosols perturbed the local temperature and circulation, which lifted the ozone layer and caused equatorial ozone depletion [Kinnison *et al.*, 1994]. Wang *et al.* [2022] reported that, in the case of the Hunga-Tonga eruption, mid-latitude ozone reduction was primarily caused by anomalous upwelling. Enhanced water can also change O₃. In the lower most stratosphere, H₂O injection through deep convection or tropopause cirrus clouds could change the catalytic chlorine/bromine free-radical chemistry and shift the total available inorganic chlorine towards the catalytically active free-radical form, ClO [Solomon *et al.*, 1997; Anderson *et al.*, 2012].

Evan *et al.* [2023] report observations of decreased O₃ and HCl, and increased ClO in the first week following the HTHH eruption at 20 hPa, which is related to the injected H₂O exceeding the normal range of the stratospheric variability. Here we use the Whole Atmosphere Community Climate Model version 6 (WACCM6) model [Zhu *et al.*, 2022] to analyze the dynamic and chemical contributors to this initial in-plume ozone depletion, and to understand the climate model performance. A lofting plume can bring ozone-poor tropospheric air into the stratosphere and cause in-plume low ozone values compared with the surrounding stratospheric air [Yu *et al.*, 2019]. For a submarine volcanic eruption, the in-plume air composition is not only impacted by tropospheric air, but also by the seawater, and volcanic gases (including H₂O, CO₂, SO₂, HCl, HF, H₂S, S₂, H₂, CO, and SiF₄), and volcanic minerals. For the HTHH initial plume, besides high H₂O and high SO₂, Microwave Limb Sounder (MLS) observations indicate the in-plume air carried high CO (**Figure A1**), relatively low ozone, and high ClO, compared with the surrounding air. We constrain the initial plume chemical compounds based on observational data from MLS; then analyze how stratospheric chemistry changes the plume composition. We will answer the following scientific questions:

1. What are the initial conditions in the volcanic plume?
2. What are the main causes of in-plume ozone depletion?

- 93 3. How do volcanic injections impact heterogeneous reactions that cause chlorine activation
 94 in the plume?
 95

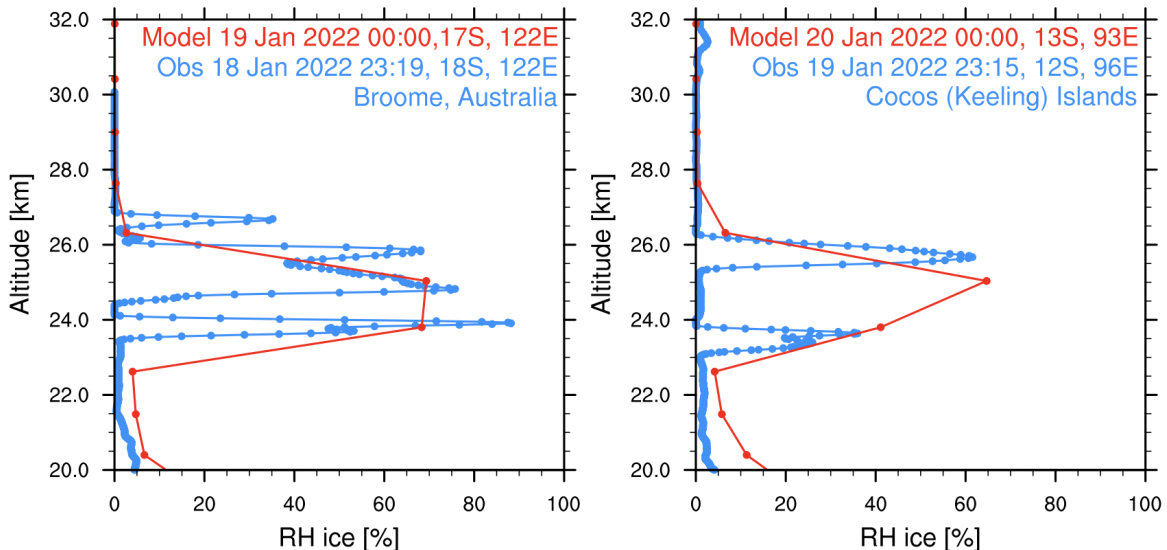
96 **2. Observational data description and model setup**

97 The MLS instrument onboard the EOS Aura satellite was launched into a near-polar sun-
 98 synchronous orbit in 2004. This work uses MLS version 4 for O₃, ClO, temperature, and CO data
 99 during the first ten days after the eruption as recommended by *Millán et al.* [2022]. The vertical
 100 resolution of these MLS products is typically around 3-5 km in the stratosphere. All data used
 101 here were screened using the methodology indicated in *Livesey et al.* [2022]. We use the MLS
 102 H₂O data to identify the plume location and define it as regions with water vapor larger than 10
 103 ppmv.

104 *Vömel et al.* [2022] provide water vapor radiosonde measurements during the first three
 105 global circumnavigations of the plume. Here we calculate the relative humidity relative to ice
 106 (RH_i) and compare the observed values with the simulated values.

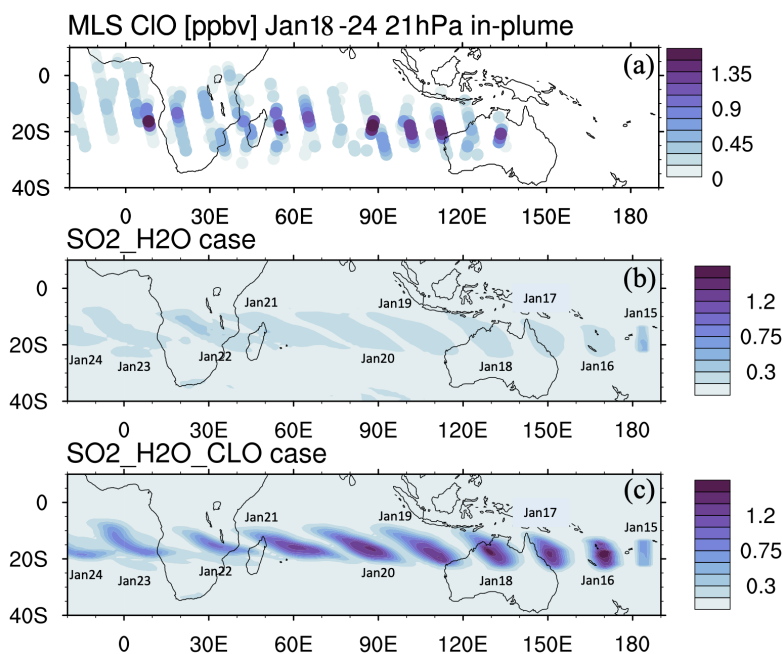
107 We use the 70-layer WACCM model as described in *Zhu et al.* [2022], injecting SO₂
 108 (0.42 Tg) and H₂O (150 Tg). The model has a horizontal resolution of 0.9° latitude × 1.25°
 109 longitude. The injection plume in the model includes about 40 grid points. The model's vertical
 110 resolution is about 1 km in the stratosphere. The model atmosphere is nudged to GEOS5
 111 MERRA meteorological analysis [*Rienecker et al.*, 2008] until January 14, one day before the
 112 eruption day. After January 15, we run the model freely with a fully interactive atmosphere and
 113 ocean for ten days.

114 We constrain the simulated volcanic aerosol, H₂O, and chlorine by comparing to
 115 observations during the first ten days after the eruption. *Zhu et al.* [2022] show that the simulated
 116 aerosol backscatter coefficient agrees with the CALIPSO observations on January 17. The
 117 simulated H₂O agrees with MLS [*Millán et al.*, 2022; *Zhu et al.*, 2022] from February 1 to April
 118 1, 2022. Here, we compare the simulated H₂O with the radiosonde observations of humidity
 119 [*Vömel et al.*, 2022] during the first week. **Figure 1** shows the RH_i on January 18 and January 19
 120 observed by the radiosonde and from nearby simulated model output. Both the observations and
 121 simulations show relative humidity between 70% to 100%. The radiosonde observations have a
 122 much higher vertical resolution than the model. Therefore, they show multiple layers of water
 123 enhancement, while the model only shows one.



125 **Figure 1.** Relative humidity with respect to ice saturation vapor pressure from radiosondes (blue)
 126 [Vömel *et al.*, 2022] and simulation (red). The profiles are picked at nearby locations. Note the
 127 observations are about 45 minutes earlier in time than the simulations, which places them on a
 128 different day.
 129

130 We constrain the chlorine injection using MLS ClO observations at 20 hPa. **Figure 2a**
 131 shows ClO from the MLS observations and the model simulations at 20 hPa from January 18 to
 132 January 24. MLS values are selected from locations where water vapor is larger than 10 ppmv,
 133 indicating these values are inside the volcanic plume. **Figures 2b** and **2c** show the simulated
 134 daytime ClO for one plume location for each day. The dates are marked next to each plume.
 135 MLS observations show elevated ClO, about 5 to 10 times higher than the ambient values
 136 (**Figure 2a**). If we only inject SO₂ and H₂O (The H₂O_SO₂ case defined in Table 1), we get a
 137 ClO amount about twice as large as the background (**Figure 2b**), which is much lower than
 138 observed. The change of ClO indicates that H₂O alters the Cly partitioning. To match the
 139 observed values, we need to inject 0.0013 Tg of ClO (**Figure 2c**). This is equivalent to injecting
 140 ~0.0009 Tg of HCl (**Figure A2**). In our simulations, injecting ClO and HCl does not lead to
 141 different HOCl (**Figure A3**), ClO, and O₃ levels after January 15, indicating the balancing of
 142 ClO and HCl inside the HTHH plume happens very quickly. Unfortunately, the HOCl retrieval
 143 from MLS is not suitable for scientific use at this pressure level, so we cannot validate it. We
 144 choose the ClO injection case in our following analysis. Note that the MLS ClO vertical
 145 resolution is ~2 km near 20 hPa, which is coarser than the model vertical resolution (~1 km at 20
 146 hPa).
 147



148 **Figure 2. a)** MLS in-plume ClO observations from January 18 - 24. “In-plume” is defined as the
 149 area with water vapor mixing ratios larger than 10 ppmv. MLS in-plume ClO data is not
 150 recommended for scientific use until January 18, 2022. **b)** and **c)** Simulated 10-day evolution of
 151 in-plume ClO in the SO₂_H₂O and SO₂_H₂O_ClO case. The modeled ClO concentrations are
 152 only taken during daytime each day (either 6 UTC or 12 UTC).
 153
 154

155 To investigate the O₃ decrease and its related chemical evolution during the first 10 days,
156 we conduct several simulations as described in **Table 1**.

157

158 **Table 1.** Model cases description.

| Name | Description |
|-------------------|--|
| Nonvolc | No injection of volcanic H ₂ O and SO ₂ . |
| H2O_SO2 | H ₂ O and SO ₂ injection profile follows Zhu et al. [2022]. |
| H2O_SO2_CIO | Besides H ₂ O and SO ₂ , injection of 0.00013 Tg of ClO. ClO injection profile is proportional to H ₂ O injection. |
| H2O_SO2_CIO_nohet | Same setting as H2O_SO2_CIO, but turn off the heterogeneous chemical reactions for HCl+HOCl, ClONO ₂ +H ₂ O, and ClONO ₂ +HCl |
| SO2_CIO | SO ₂ injection profile follows Zhu et al. (2022). No water injected. Injection of 0.00013 Tg of ClO using the same profile as H2O_SO2_CIO. |
| lowO3 | Reduce the O ₃ to 75% of its original value at 20 hPa. |
| H2O_SO2_lowO3 | H ₂ O and SO ₂ injection, plus reducing O ₃ to 75%. |
| H2O_SO2_CIO_lowO3 | H ₂ O, SO ₂ and ClO injection, plus reducing O ₃ to 75%. |
| H2O_SO2_NO | Injection of 0.003 Tg of NO in addition to H ₂ O and SO ₂ . |

159

160

161 3. Results

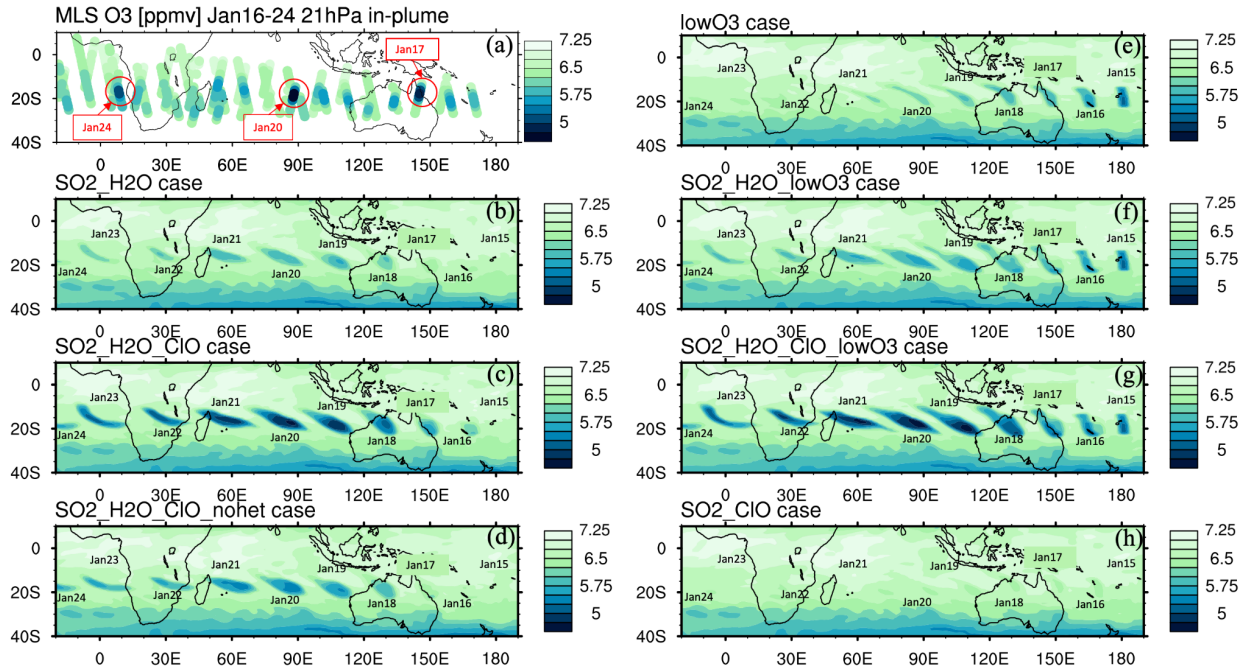
162 *Evan et al.* [2023] show the HTHH in-plume ozone depletion at 20 hPa lasts at least ten
163 days after the HTHH eruption, which they attribute to the heterogeneous chlorine activation on
164 humidified volcanic aerosols. Here we analyze the contributions to this initial in-plume O₃
165 depletion considering three processes: 1) increasing H₂O injection may enhance the HOx
166 catalytic cycle and HOx/ClOx interactions; 2) increasing ClO during the injection phase may
167 deplete ozone due to both heterogeneous reactions and gas phase reactions; 3) the rising plume
168 from the troposphere may carry ozone-poor tropospheric air into the stratosphere.

169 MLS observed in-plume low ozone concentration at 20 hPa (**Figure 3a**), especially
170 during these three days: ozone concentrations of 4.8 ppmv on January 17, 4.6 ppmv on January
171 20, and 5.1 ppmv on January 24. These are ozone anomalies of about 1.7 ppmv, 1.9 ppmv, and
172 1.4 ppmv, respectively. The anomalies are calculated using the background average values in this
173 area (6.5 ppmv) subtracting the low ozone values. Note that any interpretation of these O₃
174 anomalies needs to consider the coarse MLS vertical resolution (~3 km). Because the plume is
175 spatially small during the initial days, MLS tracks do not capture the maximum plume
176 perturbation every day. The simulation with the water injection (**Figure 3b**) accelerates the HOx
177 catalytic cycle and shows evident O₃ reduction, but less than observed. Once we inject ClO on
178 top of the massive water injection (**Figure 3c**), O₃ loss is significantly enhanced and is close to
179 the observations after January 18. The difference between **Figure 3d** and **Figure 3c** is caused by
180 heterogeneous reactions, which usually only happen in the stratospheric polar springtime where
181 they cause the Antarctic ozone hole and Arctic ozone depletion. Heterogeneous reactions
182 become important, despite the high non-polar temperatures because of the massive quantity of
183 water injected. The heterogeneous reaction rate is strongly related to the relative humidity [Shi et

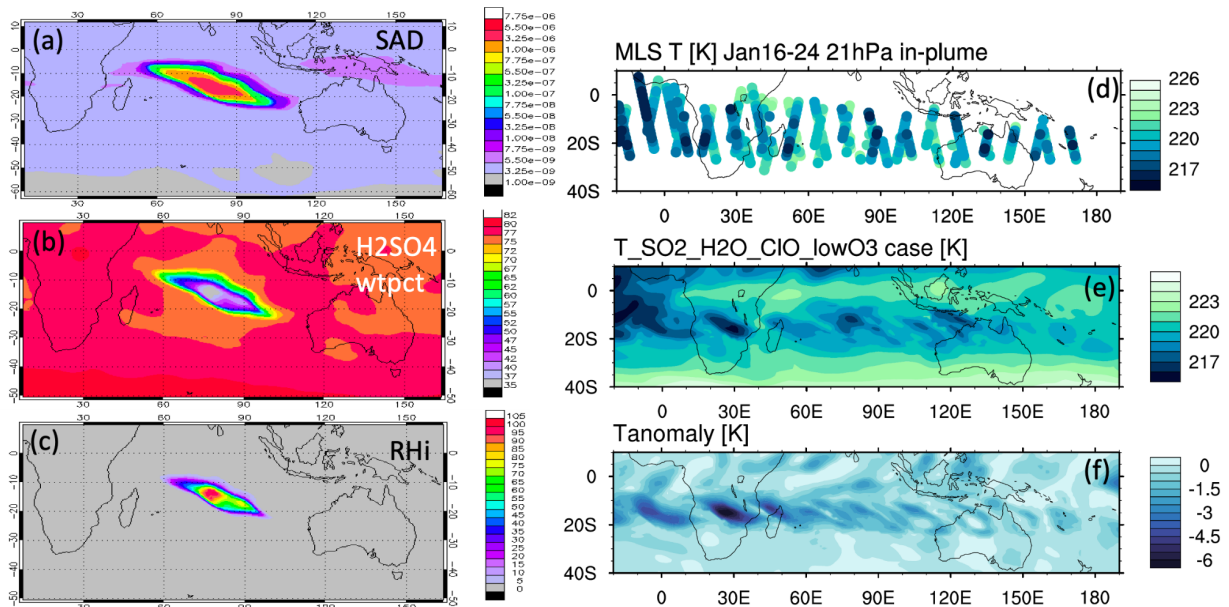
184 al., 2001]. Usually, during the polar night, the relative humidity is higher (RH_i 60%-100%) than
185 in the non-polar stratosphere because of the low temperature (<195 K). Here, the water injection
186 increases the relative humidity (**Figure 4c**). Enhanced water causes the weight percent of H₂SO₄
187 of the sulfuric acid aerosol to decrease from 70% to 35% (**Figure 4b**). The massive water
188 injection also causes the in-plume temperature to drop about 2 to 6 K (**Figure 4f**) [Solomon et
189 al., 2016]. All these factors (temperature decrease, relative humidity increase, and particle H₂SO₄
190 dilution) can increase the three heterogeneous reaction probabilities (HCl+HOCl, ClONO₂+H₂O,
191 and ClONO₂+HCl). As shown in **Figure 5**, when the water vapor amount is near the
192 climatological value of 6 ppmv, the heterogeneous reaction probability reaches 10⁻² to 10⁻¹ when
193 the temperature is ~190 K. Meanwhile, the reaction probability is similar for temperatures of 215
194 K when the water vapor is ~600 ppmv in the simulations, as was the case for the HTHH plume
195 during the week following the eruption. COSMIC-2 radio occultation observed even higher
196 water vapor during the first week: the maximum values over January 20-22 are ~1000-2000
197 ppmv [Randel et al., 2023]. Also, because the in-plume and the out-of-plume chemical
198 concentrations are different, we apply both conditions (solid and dashed lines) to show how the
199 different HCl, HOCl, and ClONO₂ conditions alter the HCl+HOCl and ClONO₂+HCl reactions
200 probabilities by one order of magnitude. Volcanic sulfur injection also increases the sulfate
201 surface area density (**Figure 4a**) that provides extra surfaces for heterogeneous reactions.

202 Comparing **Figure 3b** and **3c** with MLS observations, we can see that the chemical
203 reactions do not explain the O₃ loss during the first three days of the eruption (January 15 -
204 January 17, low O₃ near 160°E in MLS observation). This discrepancy suggests that the plume
205 contains some ozone-poor tropospheric air after the injection into the stratosphere. We ran three
206 cases with initial low ozone. For the low O₃ case (**Figure 3e**), we inject only ozone-poor air
207 without volcanic H₂O and SO₂. It shows low O₃ as observed during the first couple of days, but
208 ozone recovers quickly because the O₃ chemical lifetime is short at 20 hPa inside the plume
209 (**Figure A4**). The H₂O_SO₂_lowO₃ case (**Figure 3f**) shows ozone loss similar to the
210 observation in the first six or seven days. By adding the ClO and initial ozone-poor air (**Figure**
211 **3g**), we obtain persistent low O₃ values that agree with the observational lowest values better
212 than the other cases (**Figure 6a**). Compared with **Figure 3b**, **Figure 3d** has slightly more ozone
213 depletion, indicating that the extra chlorine injection impacts O₃ even without heterogeneous
214 chemistry. However, without including the high amounts of injected water, the additional ClO
215 alone cannot deplete ozone much (**Figure 3h**).

216

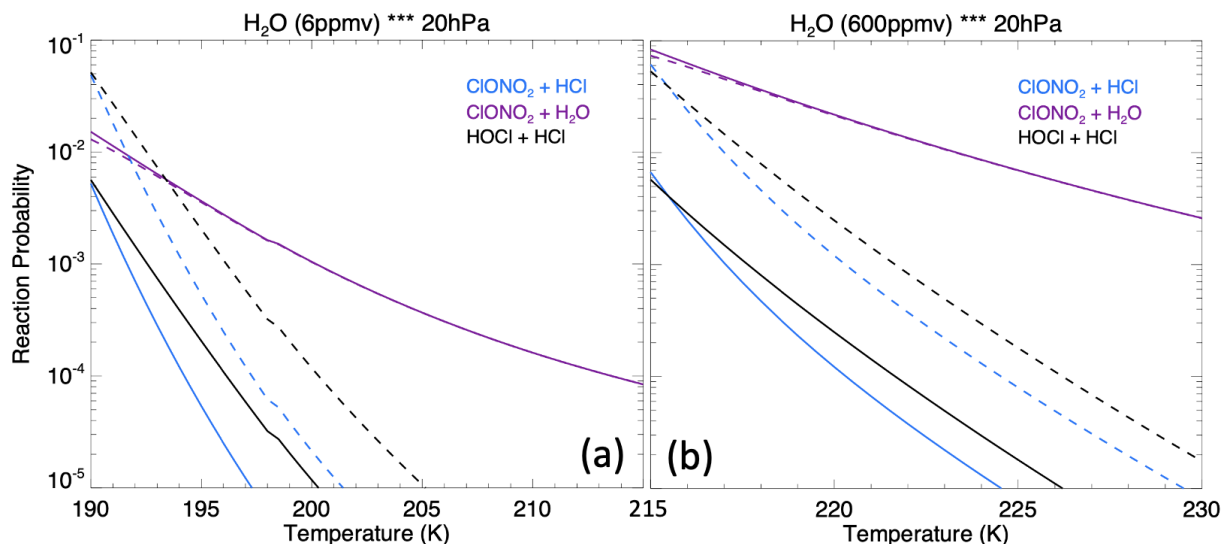


217
 218 **Figure 3.** a) MLS in-plume O₃ observation from January 16 - 24. “In-plume” is defined as in
 219 Figure 2. Note that MLS ozone retrievals were unaffected by the plume leading to the addition of
 220 two extra days of data for this figure. The locations and days with low O₃ values used in **Figure**
 221 **6** are marked with circles. **b-h)** Simulated 10-day evolution of in-plume O₃ in seven model cases
 222 with various injections of SO₂, H₂O, ClO, and low initial O₃. **Figure 3d** uses the same injection
 223 as **Figure 3c** but with heterogeneous reactions (i.e., HCl+HOCl, ClONO₂+H₂O, and
 224 ClONO₂+HCl) turned off. The simulated O₃ in the H₂O_SO₂ case uses one model time step
 225 each day that occurs near local noon.
 226



227
 228 **Figure 4.** a) Simulated surface area density, b) simulated H₂SO₄/H₂O weight percent and c)
 229 relative humidity on January 20 at 20 hPa. d) Temperature evolution during the first ten days at

230 20 hPa from MLS, **e)** simulated temperature evolution in the SO2_H2O_CIO_lowO3 case; **f)**
 231 temperature difference between the SO2_H2O_CIO_lowO3 case and the Nonvolc case.
 232



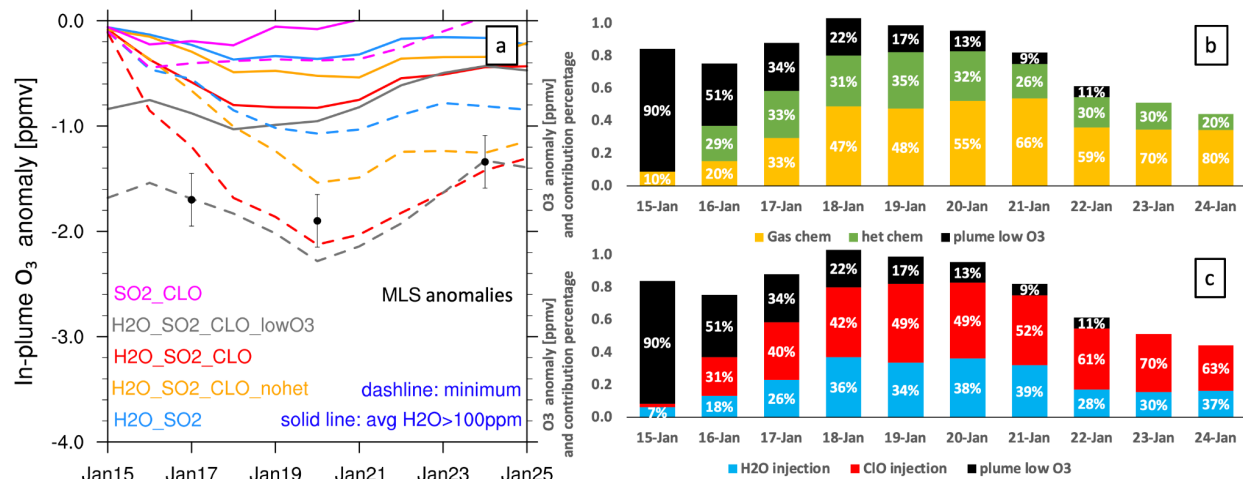
233
 234 **Figure 5.** The heterogeneous reaction probability for three reactions on sulfate surfaces
 235 ($\text{ClONO}_2 + \text{HCl}$, $\text{ClONO}_2 + \text{H}_2\text{O}$ and $\text{HOCl} + \text{HCl}$) as a function of water vapor assuming $0.4 \mu\text{m}$
 236 particle size at 20 hPa. Panel **a)** assumes 6 ppmv of ambient water vapor and panel **b)** assumes
 237 600 ppmv of ambient water vapor. The solid lines use the out-of-plume chemical concentration
 238 on January 20: 1.0 ppbv of HCl, 0.03 ppbv of HOCl, and 0.5 ppbv of ClONO_2 ; the dashed lines
 239 use the in-plume chemical concentration: 0.1 ppbv of HCl, 1.0 ppbv of HOCl, and 0.05 ppbv of
 240 ClONO_2 . These values are based on the simulation output.

241
 242 **Figure 6** shows the O_3 anomaly evolution from several model cases (**a**) and percentage
 243 contributions to the total ozone loss (**b**, **c**). The model case with all injections (initial low O_3 ,
 244 high H_2O , and high ClO) agrees well with MLS observations on the three days with the lowest
 245 O_3 values (**Figure 6a**). In **Figure 6b** and **6c**, the black bars represent the contribution from the
 246 low O_3 injection, which is significant during the first couple of days but diminishes quickly.
 247 From these percentage values, we conclude that the low O_3 carried in the plume lofting cannot be
 248 the reason for the low O_3 values after 3 days. Chemistry is the main reason that this O_3 depletion
 249 lasts so long.

250 There are two ways to look at the chemical contributors to ozone loss based on our model
 251 runs. The first is to separate the contributors due to various injections (**Figure 6c**): H_2O injection
 252 accounts for about 30-40% of the ozone loss most of the time (blue) and ClO injection accounts
 253 for 50% of the ozone loss most of the time (red). However, we cannot simply attribute the largest
 254 contribution to the ClO injection, because if we only inject ClO, it does not produce much ozone
 255 depletion (**Figure 6a**, magenta). It is the ClOx/HOx interactions that accelerate O_3 depletion.

256 A second way to look at the causes for ozone loss is to separate the contributions from
 257 the gas-phase chemistry and the heterogeneous chemistry (**Figure 6b**). The model run with the
 258 H_2O and ClO injections, but without the heterogeneous chemistry shows that the gas-phase
 259 chemistry (yellow bars) account for more than 47% of the ozone loss from January 18 - 24.
 260 Heterogeneous chemistry (green bars) destroys about 30% of the ozone. Hence, both
 261 heterogeneous chemistry and gas-phase chemistry are important for O_3 depletion. Once we turn

262 off the heterogeneous chemistry, the partitioning between active chlorine and chlorine in the
 263 reservoirs is changed. The order in which the processes are accounted for can affect the resulting
 264 breakdown. Thus, we cannot simply say that gas phase chemistry contributions are larger than
 265 heterogeneous chemistry. Both are clearly significant.
 266



267
 268 **Figure 6. a)** O₃ anomaly in different model cases. The solid lines are the average O₃ anomaly at
 269 20 hPa on each day near local noon where water vapor is larger than 100 ppmv. 100 ppmv here
 270 is suggested by *Evan et al.* [2023], who found that O₃ anomalies are not significant for a 10
 271 ppmv but significant for a 100 ppmv threshold. The dashed lines are the simulated maximum O₃
 272 anomaly on each day at 20 hPa. The black dots show the three days during which MLS measures
 273 the lowest O₃ values (explained in **Figure 3a**). **b)** The percentage contributions to ozone loss
 274 from gas phase chemistry (orange) (H₂O_SO₂_CLO_nohet), heterogeneous chemistry (green,
 275 H₂O_SO₂_CLO minus H₂O_SO₂_CLO_nohet), and low O₃ air carried into the stratosphere
 276 (black, H₂O_SO₂_CLO_lowO₃ minus H₂O_SO₂_CLO). **c)** The percentage contributions to
 277 ozone loss from H₂O injection (blue, H₂O_SO₂ minus Nonvolc), ClO injection (red,
 278 H₂O_SO₂_CLO minus H₂O_SO₂), and low O₃ air carried into the stratosphere (black,
 279 H₂O_SO₂_CLO_lowO₃ minus H₂O_SO₂_CLO).
 280

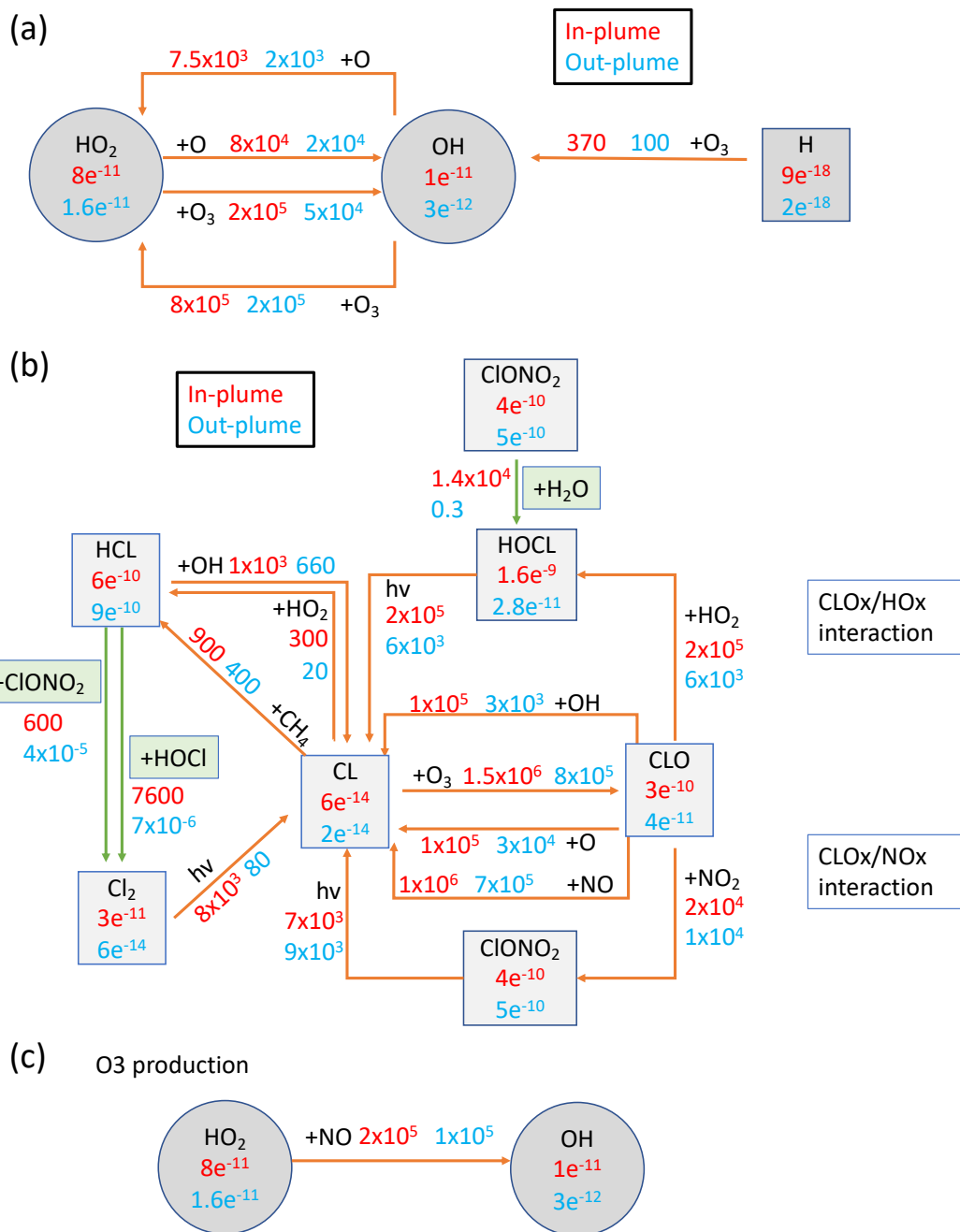
281 To better understand which reactions are critical in the HTHH plume, we investigate the
 282 simulated reaction rates related to HOx and chlorine compounds (**Figure 7**). These reactions
 283 reflect how the water and ClO injections strengthen the in-plume HOx/ClOx interactions,
 284 chlorine activation, and the relative importance of each heterogeneous reaction rate. The
 285 WACCM model uses the methods developed by *Shi et al.* [2001] for heterogeneous reaction rate
 286 calculations. **Figure 7a** shows the HOx cycle inside and outside the water plume on January 20,
 287 daytime, at 20 hPa. The HO₂+O₃ reaction rate increases by a factor of four (from 5x10⁴ to 2x10⁵
 288 cm⁻³sec⁻¹); OH+O increases by a factor of ~four (from 2x10⁴ to 7.5x10⁴ cm⁻³sec⁻¹); HO₂+O
 289 increases by a factor of four (from 2x10⁴ to 8x10⁴ cm⁻³sec⁻¹). In addition, the extra HOx plays a
 290 large role in chlorine activation. **Figure 7b** shows the chlorine compound reactions inside the
 291 HTHH initial plume. The HOCl photolysis rate increases by a factor of ~30 inside the plume
 292 (from 6x10³ cm⁻³sec⁻¹ outside the plume to 2x10⁵ cm⁻³sec⁻¹) due to the high HOCl mixing ratio,
 293 which is the dominant process causing the increase in chlorine activation to Cl. The HOCl
 294 concentration remains high due to the enhanced ClOx/HOx interaction (i.e.,
 295 ClO+HO₂→HOCl+O₂ reaction), as well as the increase of the heterogeneous reaction rate of

296 ClONO₂+H₂O by five orders of magnitude (from 0.3 to 1x10⁴ cm⁻³sec⁻¹). The large amounts of
297 HOCl also make the heterogeneous reaction of HOCl+HCl faster than the ClONO₂+HCl
298 reaction, while the latter reaction is known as the major reaction contributing to the chlorine
299 activation that contributes to the polar ozone depletion. **Figure A5** shows the uptake coefficient
300 for the three heterogeneous reactions HCl+HOCl, ClONO₂+H₂O, and ClONO₂+HCl on January
301 20. The reaction probability of ClONO₂+HCl is increased by eight orders of magnitude (from the
302 background value of 10⁻¹⁰ to 10⁻²). This value is even higher than *Evan et al.* [2023] suggested,
303 who estimate that enhanced water increases the uptake coefficient of ClONO₂+HCl to 10⁻⁴ cm⁻³
304 sec⁻¹. The reaction probability of HCl+HOCl and ClONO₂+H₂O increases to 10⁻². Furthermore,
305 inside the plume, the reactions that convert Cl back to HCl are slower than their activation rate.

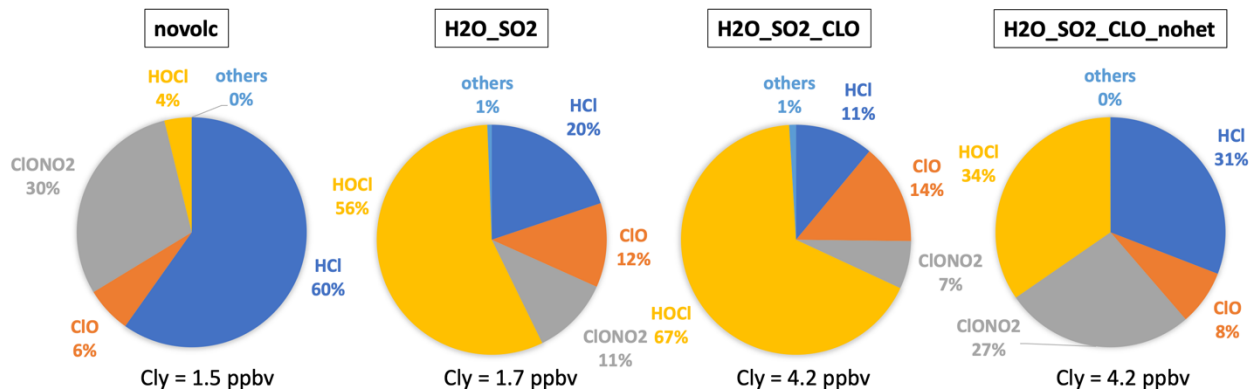
306 Besides the ozone loss reactions, ozone production reactions are also significantly altered
307 by the water plume (**Figure 7c**). HO₂+NO is usually not an important process for O₃ production
308 in the stratosphere (more important in the troposphere). The reaction rate doubles inside the
309 plume (from 1x10⁵ cm⁻³sec⁻¹ to 2x10⁵ cm⁻³sec⁻¹). Note that we don't inject lightning NO_x in this
310 case, a possible scenario during the eruption phase, that can also further increase the O₃
311 production (detailed in the discussion section).

312 Comparing the partitioning of Cly
313 (Cl+ClO+2Cl₂+2Cl₂O₂+OCIO+HOCl+ClONO₂+HCl+BrCl) reveals the in-plume chlorine
314 activation processes (**Figure 8**). Outside the plume, HCl and ClONO₂ are dominant, indicating
315 that most of the Cl is in reservoirs. While inside the water plume, both the H₂O_SO₂ and
316 H₂O_SO₂_ClO cases show strong depletion of the reservoirs HCl and ClONO₂, and most of the
317 Cly is either in the form of HOCl (a short-lived reservoir) or is activated in the form of ClO.
318 Unlike the chlorine activation process in the polar winter, HOCl is the highest in the HTHH
319 plume because heterogeneous chemistry is not fast enough to destroy HOCl to produce ClO. In
320 the case without heterogeneous chemistry, HCl and ClONO₂ are dominant in the plume,
321 indicating that heterogeneous chemistry is the main process of converting HCl to active chlorine.
322 Comparing total Cly and ClO in all panels, ClO does not exceed a quarter of the Cly, indicating
323 adding 0.00013Tg of ClO through injection is one way to produce the observed ClO. There is a
324 possibility that ClO is converted from other Cly species through chemical reactions we are not
325 aware of because this was a very unusual eruption.

326



327
 328 **Figure 7.** Reactions inside and outside the plume in $\text{cm}^{-3}\text{sec}^{-1}$ and compound concentrations in
 329 mol/mol. Red numbers represent values inside the plume, blue numbers outside the plume. **a)**
 330 HOx balance and its interaction with Ox during daytime at 20 hPa on January 20, 2022. **b)**
 331 Chlorine compound reactions in the H₂O_SO₂_ClO case. **c)** HOx cycle impact on O₃
 332 production. Green arrows represent the heterogeneous reactions for chlorine activation. H₂O is ~
 333 600 ppm inside the plume and ~5.5 ppm outside the plume. Cly is ~ 4.2 ppbv inside the plume
 334 and 1.5 ppbv outside the plume.
 335



336
 337 **Figure 8.** The percentage of each inorganic chlorine compound
 338 ($Cly = Cl + ClO + 2Cl_2 + 2Cl_2O_2 + OCIO + HOCl + ClONO_2 + HCl + BrCl$) inside and outside the plume.
 339 The slight difference between novolc Cly and H2O_SO2 Cly is because H₂O injection changes
 340 the plume dynamics in the free-running simulations.

341
 342 **4. Discussion**

343 The ozone loss inside the HTHH plume during the first ten days provides a unique
 344 opportunity to study stratospheric chemistry and to understand the performance of the WACCM
 345 state-of-the-art climate model, because the HTHH injected ClO and H₂O exceed the normal
 346 range of the stratospheric variability. These volcanic injections strongly altered the ClO_x/HO_x
 347 interactions and heterogeneous reaction rates, producing different chemical pathways for
 348 chlorine activation and ozone depletion from what occurs in the Antarctic ozone hole or Arctic
 349 ozone depletion in the polar stratospheric winter and spring. HOCl is identified as playing a large
 350 role in the in-plume chlorine balance and heterogeneous processes. The high HOCl
 351 concentrations are a result of the very high in-plume water vapor content, which makes this event
 352 different from chemistry in the Antarctic ozone hole, where ClONO₂ is more important.

353 This study also raises an interesting question of where the Cl comes from in the volcanic
 354 injection. Seawater contains 3.5% sea salt, which implies that about 5 Tg of NaCl could have
 355 been injected assuming that the injected 150 Tg of H₂O came from sea water. However, we only
 356 need to inject 0.00013 Tg of ClO to match the MLS ClO observations during the first few days
 357 after the eruption. We also conducted a test injecting an equivalent amount of HCl (0.0009 Tg),
 358 which resulted in a similar HOCl, ClO, and O₃ pattern (**Figure A2 and A3**). If we inject more
 359 HCl or ClO, ClO would exceed the observed concentration, causing depletion of OH, and
 360 slowing down the SO₂ oxidation. Evidently, if the water came from seawater, most NaCl was not
 361 converted to HCl but stayed in the stratosphere as particles. *Vernier et al.* [2023] sampled NaCl
 362 particles eight months after the eruption near Brazil. Based on their sampled NaCl concentration,
 363 we estimate 0.5 to 1 Tg of NaCl may have been injected and stayed in the atmosphere. There are
 364 several possibilities why this event did not inject 5 Tg of NaCl in the stratosphere: Remote
 365 sensing particle size estimations [*Khaykin et al.*, 2022] and in-situ measurements [*Asher et al.*,
 366 2023] indicates that the particles were submicron sized. However, sea salt particles injected into
 367 the lower troposphere by wind are mainly particles larger than 10 μm. Hence, if the volcanic
 368 injection had similar sized NaCl particles, most of them may have quickly fallen out of the
 369 stratosphere. In addition, the majority of NaCl might have been washed out during the first
 370 couple of hours of plume injection by acting as nuclei for ice particles. It is also possible that the
 371 reactions that might release Cl from NaCl may not efficiently lead to reactive Cl. For example,
 372 HNO₃ can react on sea salt heterogeneously very quickly in the troposphere to release HCl (De

373 Haan and Finlayson-Pitts, 1997; Guimbaud et al., 2002; Murphy et al., 2019). This reaction may
374 be accelerated by HTHH high humidity even if the temperature is low in the stratosphere. HCl
375 could be removed by condensing in supercooled water, which would reduce HCl vapor
376 concentrations by up to four orders of magnitude, preventing substantial stratospheric chlorine
377 injection [Tabazadeh and Turco, 1993]. Finally, it may be that the water injected came from
378 magmatic water, or seawater that percolated into the volcano and was released as steam. Such
379 water would not be rich in NaCl. In that case Cl observed by Vernier et al. [2023] may have been
380 bound up in minerals of the volcanic ash. Other halogen species such as bromine and iodine are
381 often observed after volcanic eruptions (large amounts of BrO were observed after HTHH in the
382 troposphere [Li et al., 2023]). However, they can lead to much stronger ozone depletion if they
383 persist in the stratosphere. Since the elevated Cl in the model can well explain the O₃ depletion,
384 the impact of bromine and iodine on stratospheric O₃ is minimal for this eruption.

385 In addition, NO_x can be produced by lightning inside or around the volcanic plume.
386 Observations show there was a record number of lightning events in this volcanic plume. Almost
387 400,000 flashes were observed by the GLD360 network over the 6 hours of the most active
388 eruption period (and ~590,000 total flashes) [Global Volcanism Program, 2022]. Considering
389 that tropospheric global models use a lightning source of 5 Tg(N)/yr and an average flash the
390 OTD/LIS satellite sensors produced an average global flash rate of 44±5 flashes per second, an
391 injection of N of ~0.001- 0.003 Tg (0.002 - 0.006 Tg of NO) would be expected for the HTHH
392 eruption. We conducted a model run with H₂O, SO₂, and an injection of 0.003 Tg of NO (the
393 H₂O_SO₂_NO case), showing that this additional NO has little impact on the O₃ loss and ClO
394 levels during the first ten days (**Figure A6**). Compared to the H₂O_SO₂ case, the simulated O₃
395 loss in the H₂O_SO₂_NO case increased by ~ 5x10⁵ molecules/cm³/sec, but at the same time,
396 the O₃ production rate increased by ~ 5x10⁵ molecules/cm³/sec. The NO+HO₂ reaction rate in
397 the H₂O_SO₂_NO case increases 5 times compared with the H₂O_SO₂ case. Therefore, lightning
398 NO_x probably does not contribute to the HTHH initial in-plume O₃ loss. Because of the high
399 water, NO would convert to HNO₃ in the first couple of days. Unfortunately, we lack
400 observations of HNO₃, NO, or NO₂ right after the eruption. MLS observations in February
401 (**Figure A7**) and the model simulations with H₂O injection or H₂O+NO injections show elevated
402 HNO₃ compared with the background.

403
404
405
406

Appendix A is provided in a separate file.

407 **Code availability:** The CESM2 model is available on the CESM trunk to any registered user at
408 www.cesm.ucar.edu.

409 **Data availability:** The main simulation data generated during this study are available at
410 (<https://osf.io/f69ns/>) with a permanent DOI 10.17605/OSF.IO/F69NS. Aura MLS v4 data is
411 available at <https://disc.gsfc.nasa.gov/datasets?page=1&keywords=AURA%20MLS>. Water
412 vapor radiosonde data is available at <https://doi.org/10.5065/p328-z959> (26).

413 **Author contribution:** YZ, RWP, DK, and KHR designed the experiments and YZ performed
414 the simulations. YZ prepared the manuscript with contributions from all co-authors. DK
415 examined the sensitivity of the stratospheric H₂O abundance on the reaction probability (Figure

416 5). LM, HV and SE provided observational data and analysis. RWP, DK, OBT, JZ, ST, CGB,
417 XW, WJR and KHR participated in the modeling data analysis.

418 **Competing interests:** At least one of the (co-)authors is a member of the editorial board
419 of Atmospheric Chemistry and Physics.

420

421 **Acknowledgement**

422 This project received funding from NOAA's Earth Radiation Budget (ERB) Initiative
423 (CPO #03-01-07-001). This research was supported in part by NOAA cooperative agreements
424 NA17OAR4320101 and NA22OAR4320151. We thank Hazel Vernier, Dr. Kimberlee Dube, Dr.
425 Pengfei Yu, Fracis Vitt, Dr. Ru-shan Gao, Dr. Margaret Tolbert, Dr. Micheal Mills, Dr. Daniel
426 Murphy, and Dr. Brian Ridley for their valuable input. NCAR's Community Earth System
427 Model project is supported primarily by the National Science Foundation. This material is based
428 upon work supported by the National Center for Atmospheric Research, which is a major facility
429 sponsored by the NSF under Cooperative Agreement No. 1852977. Computing and data storage
430 resources, including the Cheyenne supercomputer (doi:10.5065/D6RX99HX), were provided by
431 the Computational and Information Systems Laboratory (CISL) at NCAR. Work at the Jet
432 Propulsion Laboratory, California Institute of Technology, was carried out under a contract with
433 the National Aeronautics and Space Administration (80NM0018D0004).

434

435

436 **Reference:**

437

- 438 Anderson, J. G., D. M. Wilmoth, J. B. Smith, and D. S. Sayres (2012), UV Dosage Levels in
439 Summer: Increased Risk of Ozone Loss from Convectively Injected Water Vapor, *Science*,
440 337(6096), 835-839, doi: <https://doi.org/10.1126/science.1222978>.
- 441 Asher, E., Todt, M., Rosenlof, K.H., Thornberry, T.D., Gao, R.S., Taha, G., Walter, P.J.,
442 Alvarez, S.L., Flynn, J., Davis, S.M. and Evan, S., (2022). The unprecedented rapid aerosol
443 formation from the Hunga Tonga-Hunga Ha'apai eruption. AGU Fall Meeting Abstracts
444 (Vol. 2022, pp. A42I-01).
- 445 De Haan, D. O.; Finlayson-Pitts, B. J. Knudsen cell studies of the reaction of gaseous nitric acid
446 with synthetic sea salt at 298 K. *J. Phys. Chem. A* 1997, 101, 9993-9999,
447 doi:10.1021/jp972450s.
- 448 Evan et al., (2023), Rapid ozone loss following humidification of the stratosphere by the Hunga
449 Tonga Eruption, accepted by Science.
- 450 Global Volcanism Program, 2022. Report on Hunga Tonga-Hunga Ha'apai (Tonga). In: Sennert,
451 S K (ed.), Weekly Volcanic Activity Report, 12 January-18 January 2022. Smithsonian
452 Institution and US Geological Survey.
- 453 Guimbaud, C.; Arens, F.; Gutzwiller, L.; Gäggeler, H. W.; Ammann, M. Uptake of HNO₃ to
454 deliquescent sea-salt particles: a study using short-lived radioactive isotope tracer ¹³N.
455 *Atmos. Chem. Phys.* 2002, 2, 249-257, doi:10.5194/acp-2-249-2002.
- 456 Hofmann, D. J., and S. J. Oltmans (1993), Anomalous Antarctic ozone during 1992: Evidence
457 for Pinatubo volcanic aerosol effects, *Journal of Geophysical Research: Atmospheres*,
458 98(D10), 18555-18561, doi:<https://doi.org/10.1029/93JD02092>.

459 Khaykin, S., et al. (2022), Global perturbation of stratospheric water and aerosol burden by
460 Hunga eruption, *Communications Earth & Environment*, 3(1), 316, doi:10.1038/s43247-022-
461 00652-x.

462 Kinnison, D. E., K. E. Grant, P. S. Connell, D. A. Rotman, and D. J. Wuebbles (1994), The
463 chemical and radiative effects of the Mount Pinatubo eruption, *Journal of Geophysical*
464 *Research: Atmospheres*, 99(D12), 25705-25731, doi: <https://doi.org/10.1029/94JD02318>.

465 Li, Q., Qian, Y., Luo, Y., Cao, L., Zhou, H., Yang, T., ... & Liu, W. (2023). Diffusion Height and
466 Order of Sulfur Dioxide and Bromine Monoxide Plumes from the Hunga Tonga–Hunga
467 Ha’apai Volcanic Eruption. *Remote Sensing*, 15(6), 1534.

468 Livesey, N., J., Read, W. G., Wagner, P. A., Froidevaux, L., Santee, M. L., Schwartz, M. J., et
469 al. (2022), Version 5.0x Level 2 and 3 data quality and description document (Tech. Rep.
470 No.JPL D-105336 Rev. B). Jet Propulsion Laboratory, Retrieved from
471 https://mls.jpl.nasa.gov/data/v5-0_data_quality_document.pdf

472 Millán, L., et al. (2022), The Hunga Tonga-Hunga Ha'apai Hydration of the Stratosphere,
473 *Geophysical Research Letters*, 49(13), e2022GL099381,
474 doi:<https://doi.org/10.1029/2022GL099381>.

475 Murphy, D. M., Froyd, K. D., Bian, H., Brock, C. A., Dibb, J. E., DiGangi, J. P., ... & Yu, P.
476 (2019). The distribution of sea-salt aerosol in the global troposphere. *Atmospheric Chemistry*
477 *and Physics*, 19(6), 4093-4104.

478 Portmann, R. W., S. Solomon, R. R. Garcia, L. W. Thomason, L. R. Poole, and M. P.
479 McCormick (1996), Role of aerosol variations in anthropogenic ozone depletion in the polar
480 regions, *Journal of Geophysical Research: Atmospheres*, 101(D17), 22991-23006,
481 doi:<https://doi.org/10.1029/96JD02608>.

482 Randel, W. J., Johnston, B. R., Braun, J. J., Sokolovskiy, S., Vömel, H., Podglajen, A., & Legras,
483 B. (2023). Stratospheric Water Vapor from the Hunga Tonga–Hunga Ha’apai Volcanic
484 Eruption Deduced from COSMIC-2 Radio Occultation. *Remote Sensing*, 15(8), 2167.

485 Rienecker, M. M. et al. The GEOS-5 Data Assimilation System: Documentation of Versions 5.0.
486 1, 5.1. 0, and 5.2. 0 (2008).

487 Shi, Q., J. T. Jayne, C. E. Kolb, D. R. Worsnop, and P. Davidovits (2001), Kinetic model for
488 reaction of ClONO₂ with H₂O and HCl and HOCl with HCl in sulfuric acid solutions,
489 *Journal of Geophysical Research: Atmospheres*, 106(D20), 24259-24274,
490 doi:<https://doi.org/10.1029/2000JD000181>.

491 Solomon, S., S. Borrmann, R. R. Garcia, R. Portmann, L. Thomason, L. R. Poole, D. Winker,
492 and M. P. McCormick (1997), Heterogeneous chlorine chemistry in the tropopause region,
493 *Journal of Geophysical Research: Atmospheres*, 102(D17), 21411-21429,
494 doi:<https://doi.org/10.1029/97JD01525>.

495 Solomon, S., D. J. Ivy, D. Kinnison, M. J. Mills, R. R. Neely, and A. Schmidt (2016),
496 Emergence of healing in the Antarctic ozone layer, *Science*, 353(6296), 269-274,
497 doi:<https://doi.org/10.1126/science.aae0061>.

498 Solomon, S., Rosenlof, K.H., Portmann, R.W., Daniel, J.S., Davis, S.M., Sanford, T.J. and
499 Plattner, G.K., 2010. Contributions of stratospheric water vapor to decadal changes in the
500 rate of global warming. *Science*, 327(5970), pp.1219-1223. DOI:10.1126/science.1182488

501 Tabazadeh, A., and R. P. Turco (1993), Stratospheric Chlorine Injection by Volcanic Eruptions:
502 HCl Scavenging and Implications for Ozone, *Science*, 260(5111), 1082-1086, doi:
503 <https://doi.org/10.1126/science.260.5111.1082>.

504 Tie, X., and G. Brasseur (1995), The response of stratospheric ozone to volcanic eruptions:
505 Sensitivity to atmospheric chlorine loading, *Geophysical Research Letters*, 22(22), 3035-
506 3038, doi:<https://doi.org/10.1029/95GL03057>.

507 Vernier, H., Quintão, D., Biazon, B., Landulfo, E., Souza, G., J. S. Lopes, F., Rastogi, N.,
508 Meena, R., Liu, H., Fadnavis, S., Mau, J., K. Pandit, A., Berthet, G., and Vernier, J.-P.:
509 Understanding the impact of Hunga-Tonga undersea eruption on the stratospheric aerosol
510 population using Balloon measurements, Satellite data, and model simulations, EGU General
511 Assembly 2023, Vienna, Austria, 24–28 Apr 2023, EGU23-6882,
512 <https://doi.org/10.5194/egusphere-egu23-6882>, 2023.

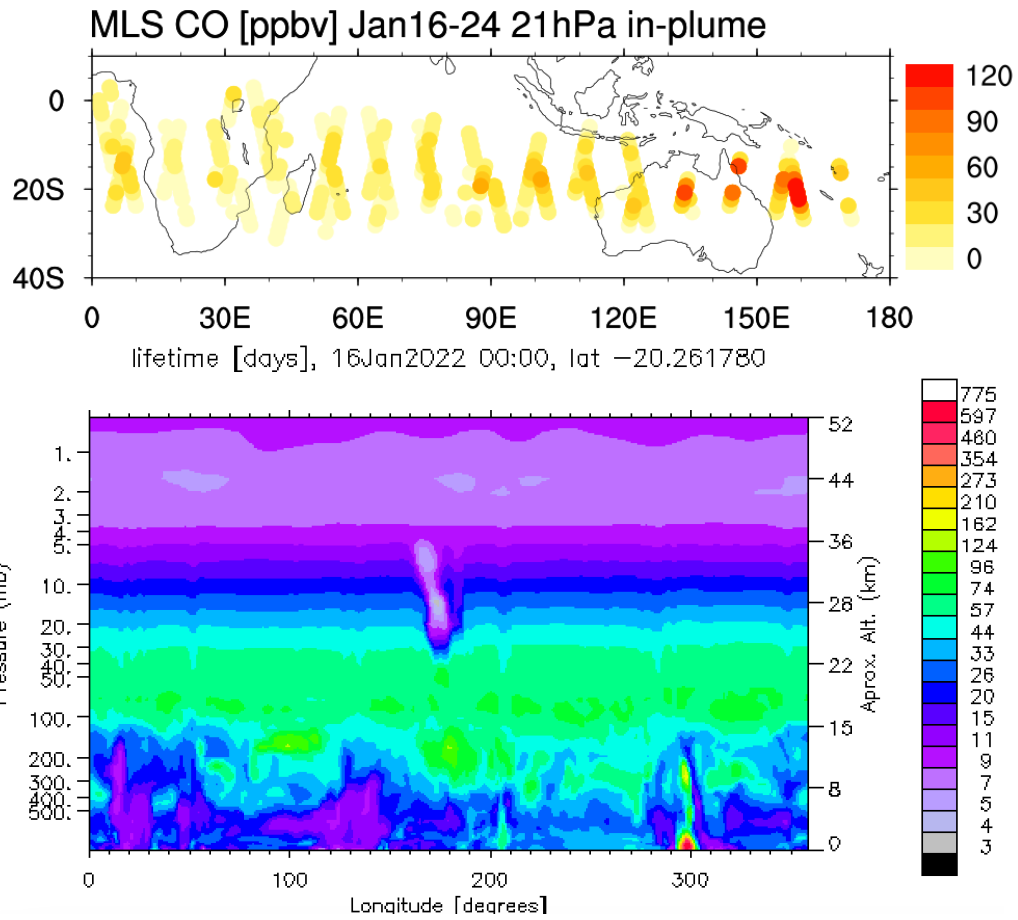
513 Vömel, H., S. Evan, and M. Tully (2022), Water vapor injection into the stratosphere by Hunga
514 Tonga-Hunga Ha’apai, *Science*, 377(6613), 1444-1447, doi:
515 <https://doi.org/10.1126/science.abq2299>.

516 Wang, X., W. Randel, Y. Zhu, S. Tilmes, J. Starr, W. Yu, R. Garcia, B. Toon, M. Park, and D.
517 Kinnison (2022), Stratospheric climate anomalies and ozone loss caused by the Hunga Tonga
518 volcanic eruption, *Authorea Preprints*.

519 Yu, P., et al. (2019), Black carbon lofts wildfire smoke high into the stratosphere to form a
520 persistent plume, *Science*, 365(6453), 587-590, doi:<https://doi.org/10.1126/science.aax1748>.

521 Zhu, Y., et al. (2022), Perturbations in stratospheric aerosol evolution due to the water-rich
522 plume of the 2022 Hunga-Tonga eruption, *Communications Earth & Environment*, 3(1), 248,
523 doi:10.1038/s43247-022-00580-w.

524
525
526

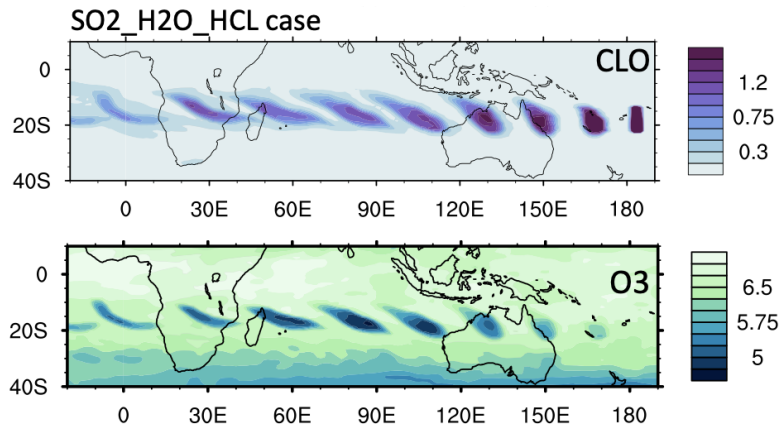


529

530

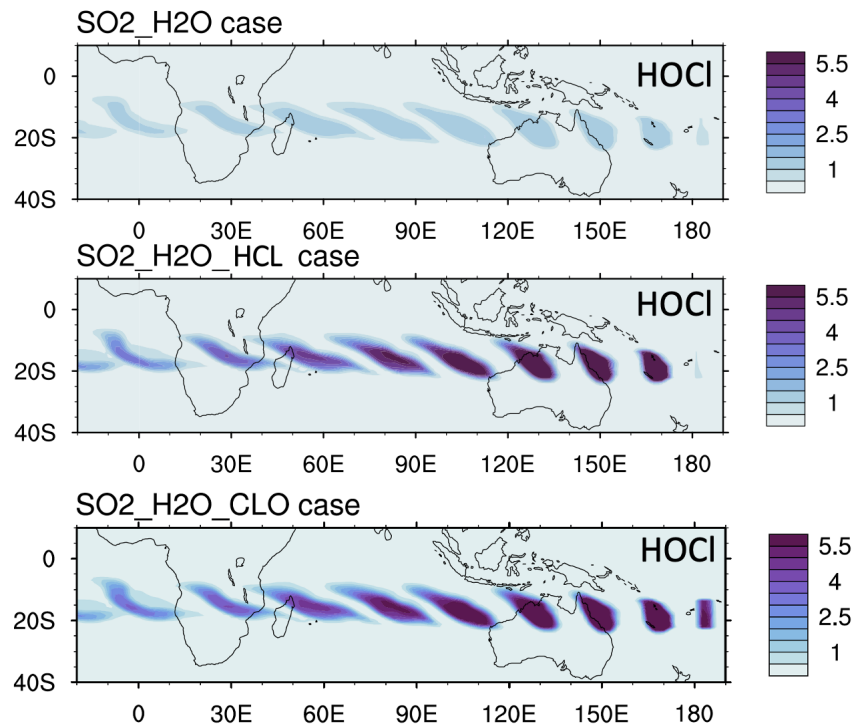
531 **Figure A1.** Top panel shows the MLS in-plume CO observation during the first 10 days after the
 532 eruption. The bottom panel shows the CO lifetime on Jan 16 at 20°S is shortened from a month
 533 to a few days because of the volcanic water plume. The observed CO mixing ratios of around
 534 120 ppmv seem incompatible with typical CO levels over oceanic regions, indicating the
 535 production of CO within the magma chamber or in the hot plume itself.

536

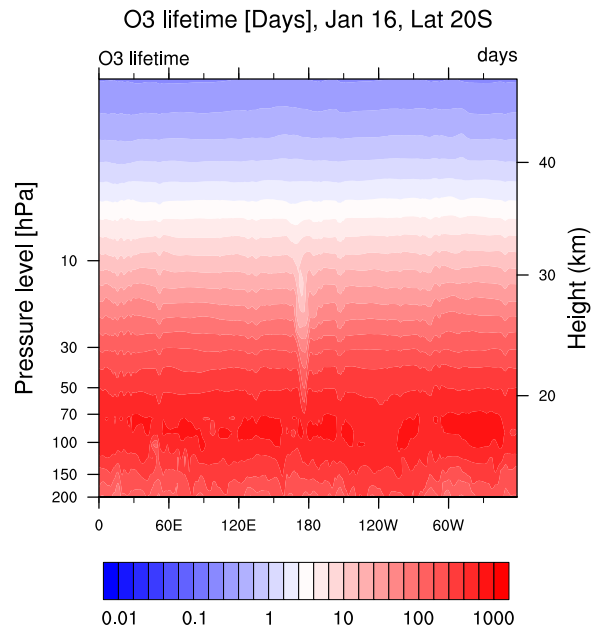


537

538 **Figure A2.** The O₃ and ClO evolution from the model case with an HCl injection of 0.000092
 539 Tg (equivalent to 0.00013 Tg of ClO injection).
 540



541 **Figure A3.** The HOCl evolution from the three model cases.
 542
 543



544 **Figure A4.** O₃ chemical lifetime is about 1 to 2 months at 20 hPa and is reduced to 10 days at the
 545 HTHH location.
 546
 547

548
549
550
551

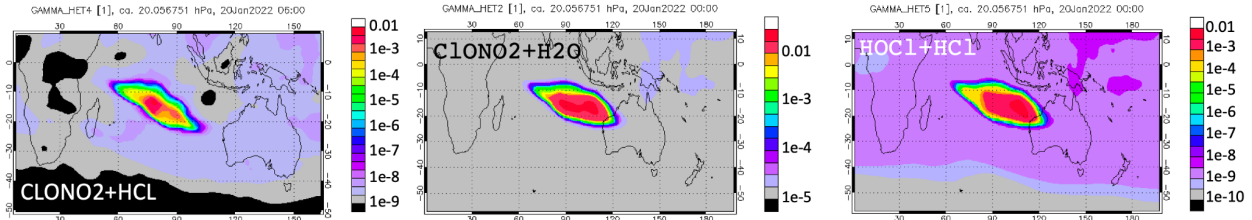


Figure A5. Heterogeneous reaction probabilities for the three heterogeneous reactions on January 20 at 20 hPa.

552
553
554
555

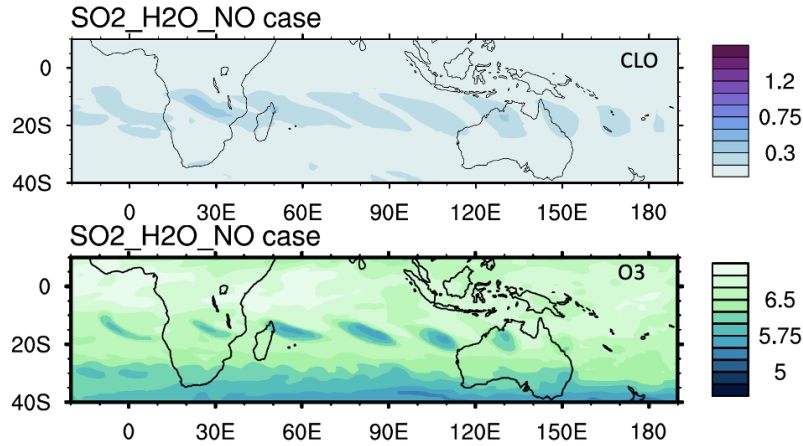
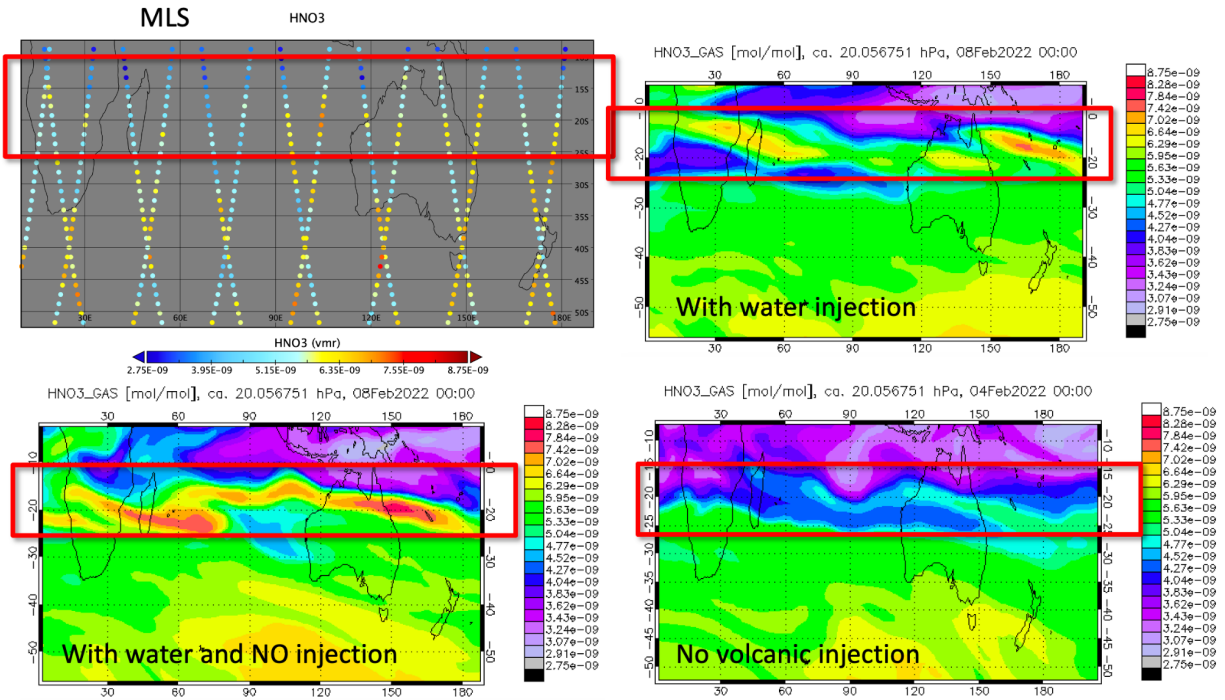


Figure A6. O₃ and ClO evolution from the model case with NO injection of 0.003 Tg, which is identical to the SO₂_H₂O case. The ClO and O₃ enhancement are due to the H₂O injection.

556



557 **Figure A7.** HNO₃ observed by MLS on February 8, 2022 compared to the model simulation
558 with water and NO injection, as well as the no volcanic injection case. MLS shows similar
559 elevated HNO₃ as the simulation case with H₂O injection or with H₂O/NO injection.
560